Next Generation Fire Severity Mapping

Primary author and contact:
Sean Parks
Aldo Leopold Wilderness Research Institute
Rocky Mountain Research Station
US Forest Service
sean_parks@fs.fed.us

Citation and further details:
Parks SA, Holsinger LM, Panunto MH, Jolly WM, Dobrowski SZ, and Dillon GK. 2018. High-severity fire: evaluating its key drivers and mapping its probability across western US forests. *Environmental Research Letters.* 13: 044037. http://iopscience.iop.org/article/10.1088/1748-9326/aab791

Abstract:
The geospatial products described and distributed here depict the probability of high-severity fire, if a fire were to occur, for several ecoregions in the contiguous western US.

The ecological effects of wildland fire – also termed the fire severity – are often highly heterogeneous in space and time. This heterogeneity is a result of spatial variability in factors such as fuel, topography, and climate (e.g. mean annual temperature). However, temporally variable factors such as daily weather and climatic extremes (e.g. an unusually warm year) also may play a key role.

Scientists from the US Forest Service Rocky Mountain Research Station and the University of Montana conducted a study in which observed data were used to produce statistical models describing the probability of high severity fire as a function of fuel, topography, climate, and fire weather. Observed data from over 2000 fires were used to build individual models for each of 19 ecoregions in the contiguous US (see Fig. 1 below). High severity fire was measured using a fire severity metric termed the relativized burn ratio, which uses pre- and post-fire Landsat imagery to measure fire-induced ecological change. Fuel included pre-fire metrics of live fuel amount such as NDVI. Topography included factors such as slope and potential solar radiation. Climate summarized 30-year averages of factors such as mean summer temperature that spatially vary across the study area. Lastly, fire weather incorporated temporally variable factors such as daily and annual temperature.

In turn, these statistical models were used to generate "wall-to-wall" maps depicting the probability of high severity fire, if a fire were to occur, for 13 of the 19 ecoregions. Maps were not produced for ecoregions in which model quality was deemed inadequate. All maps use fuel data representing the year 2016 and therefore provide a fairly up-to-date assessment of the potential for high severity fire. For those ecoregions in which the relative influence of fire weather was fairly strong (n=6), two additional maps were produced, one depicting the probability of high severity fire under moderate weather and the other under extreme weather. An important consideration is that only pixels defined as forest were used to build the models; consequently maps exclude pixels considered non-forest.

Users of these data should thoroughly read through this document to better understand appropriate uses and interpretations of the data products distributed here.

Figure 1. Of the 19 ecoregion analyzed, 13 performed at a level (AUC ≥0.70) in which we felt comfortable producing maps depicting the probability of high-severity fire. These 13 ecoregions are identified by the circle (any style) and the resulting predictions are a composite (i.e. and average) of 100 independent predictions using randomly selected fire weather. The relative influence of fire weather was ≥15% in six of these 13 ecoregions, which are identified by the double circle. These six ecoregions have two additional products, one depicting the probability of high-severity fire under moderate weather (i.e. the 50th percentile of the 100 independent predictions) and the other under extreme weather (i.e. the 95th percentile of the 100 independent predictions). See Methods for further details.

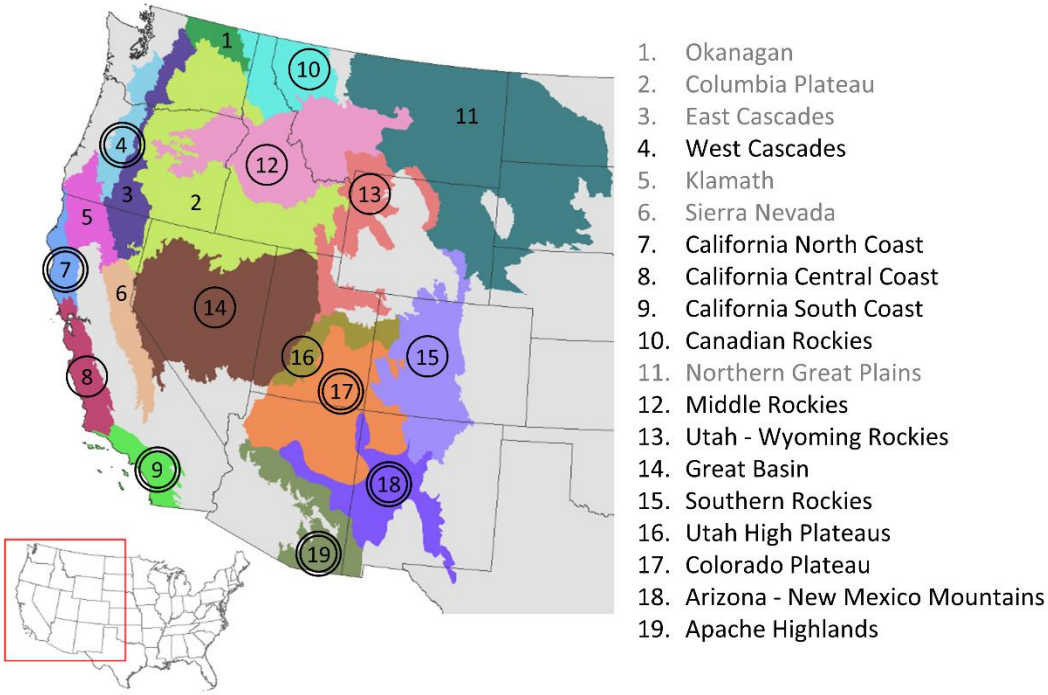

Important notes about usage:

- All mapped probabilities are conditional on a fire burning any given pixel. Simply put, these are the maps represent the probability of high-severity fire were a fire to occur.
- It is not appropriate to compare severity predictions among ecoregions because each ecoregional model was developed independently.
- Because the range and frequency distribution of high-severity fire probabilities are highly dependent on the prevalence (i.e. the proportion) of high-severity fire in each ecoregion, the probabilities should not be strictly interpreted based on a range of zero to one. This means users should not, for example, conclude that a pixel with a 0.50 probability of high-severity fire has a 50% chance of burning at high-severity. Instead, a better interpretation are relative differences in probabilities within each ecoregion. For example, a pixel with a 0.40 probability fire has twice the likelihood of burning at high-severity compared to a pixel with a 0.20 probability.

Files included with each ecoregional zip file:

1. **severity.prediction.mean.tif** – This is the pixel-wise average of 100 independent predictions using randomly drawn fire weather. See Methods. This raster is available for the 13 ecoregions indicated in Figure 1. This is located in the 'severity.predictions' directory.
2. **severity.prediction.p50.tif** – This is the 50th percentile prediction (independently calculated for each pixel) of 100 independent predictions using randomly drawn fire weather. This is intended to represent the likelihood of high-severity fire under moderate weather conditions. This raster is available for the six ecoregions indicated in Figure 1. This is located in the 'severity.predictions' directory.
3. **severity.prediction.p95.tif** – This is the 95th percentile prediction (independently calculated for each pixel) of 100 independent predictions using randomly drawn fire weather. This is intended to represent the likelihood of high-severity fire under extreme weather conditions. This raster is available for the six ecoregions indicated in Figure 1. This is located in the 'severity.predictions' directory.
4. **nonforest.mask.tif** – This raster shows what was considered forest (value=0) and nonforest (value=1) and is provided in case users want it to produce pretty maps (given we did not make predictions for nonforest pixels). This is located in the 'nonforest.mask' directory'.
5. **ecoregion_boundary.shp** – This shapefile shows the boundary for the ecoregion of interest. The original source is The Nature Conservancy (Olson and Dinerstein 2002). This is mostly provided in case users need it to produce visually appealing maps. This is located in the 'ecoregion.boundary' directory.
6. **ecoregion_boundary_reverse.shp** – This shapefile provides a 'donut' of sorts around the ecoregion of interest. This is mostly provided in case users need it to produce visually appealing maps (i.e. by masking out areas outside the ecoregion). This is located in the 'ecoregion.boundary' directory.

Resolution: 30 meter pixels

Projection:
Projected Coordinate System: Albers_Conical_Equal_Area
Projection: Albers
false_easting: 0.00000000
false_northing: 0.00000000
central_meridian: -96.00000000
standard_parallel_1: 29.50000000
standard_parallel_2: 45.50000000
latitude_of_origin: 23.00000000
Linear Unit: Meter

Geographic Coordinate System: GCS_North_American_1983
Datum: D_North_American_1983
Prime Meridian: Greenwich
Angular Unit: Degree

Methods used to develop the severity predictions (from Parks et al. 2018. High-severity fire: evaluating its key drivers and mapping its probability across western US forests. *Environmental Research Letters.* 13: 044037):

Data

We built a statistical model describing high-severity fire for each ecoregion in the western US; ecoregion boundaries were obtained from The Nature Conservancy (Olson and Dinerstein 2002) (Fig. 1). Fire severity was measured using the relativized burn ratio (RBR), a satellite index (resolution = 30-m) that differences pre- and post-fire Landsat thematic mapper (TM), enhanced thematic mapper plus (ETM+), and operational land imager (OLI) satellite data. The RBR has a high correspondence to field-based measures of severity such as the composite burn index (CBI; r^2=0.71) (Parks et al. 2014a). We classified the RBR data into binary categories representing high-severity (RBR ≥ 298) and other severity (RBR < 298). This threshold was based on a CBI value of 2.25 (Parks et al. 2014a), which corresponds to ≥ 95% canopy mortality (Miller et al. 2009). Although there is some evidence that RBR thresholds defining high-severity can vary across the US (Parks et al. 2014a), CBI data were not available to allow identification of RBR thresholds for each of the 19 ecoregions. A similar thresholding approach was also used by Dillon et al. (2011), and high-severity fire can be considered stand-replacing fire in the context of this study. Satellite imagery used to generate RBR was obtained from the Monitoring Trends in Burn Severity program (MTBS) (Eidenshink et al. 2007), which distributes Landsat data for fires ≥ 400 ha that occurred since 1984. RBR was calculated using the 'dNBR offset', which accounts for differences due to phenology or precipitation between the pre- and post-fire imagery by subtracting the average delta normalized burn ratio (dNBR) of pixels outside the burn perimeter (Key 2006); this can be important when comparing severity among fires (Parks et al. 2014a).

We evaluated 16 explanatory variables in the model for each ecoregion which can be categorized into four groups representing live fuel, topography, climate, and fire weather (Table 1). The fuel group is comprised of three satellite vegetation indices: NDVI, NDMI, and EVI (Table 1). These indices were generated using pre-fire imagery distributed by MTBS. NDVI is an index of vegetation productivity and biomass (Pettorelli et al. 2005). NDMI is a measure of vegetation moisture and is frequently used in drought monitoring, and because of its sensitivity, it is also key in assessing wildfire potential and severity (McDonald et al. 1998, Chu et al. 2016). EVI is another index of vegetation productivity, but whereas NDVI is chlorophyll sensitive, EVI is more responsive to canopy structural variations (i.e. leaf area index, canopy type, plant physiognomy, and canopy architecture) and may be better suited to high biomass regions (Huete et al. 2002). These three metrics are sensitive to changes in amounts and distribution of live fuel over time due to vegetation growth, disturbance, and drought (Turner 2010). These metrics implicitly incorporate management activities and disturbances such as fuel reduction treatments and wildland fire. Inclusion of 'static' fuel metrics such as vegetation type or cover (e.g. www.landfire.gov) (cf. Birch et al. 2015, Keyser and Westerling 2017) was not considered since such products are only updated periodically and are thus not sensitive to annual dynamics. The inclusion of dynamic fuel metrics allows for annual updates of the fire severity predictions while accounting for temporal variability in fuel.

Topography is represented by four variables (resolution = 30-m): dissection index (DISS), topographic position index (TPI), potential solar radiation (SRAD), and slope (Slope) (Table 1). DISS is a measure of roughness (i.e. a ratio between relative and absolute relief), and varies between zero (absence of dissection, e.g. low portion of a basin) and one (e.g. vertical cliff) (Evans 1972). TPI is a measure of valley bottom vs. ridge top and was calculated at the 2-km scale. SRAD incorporates slope, aspect, and topographic shading and is a measure of insolation (Flint et al. 2004). Slope is a measure of steepness. These particular topographic variables are strongly linked to fire severity (Dillon et al. 2011, Birch et al. 2015), although they most likely represent indirect processes that drive fire severity. For example, solar radiation (SRAD) may indirectly affect fire severity through its influence on productivity and fuel moisture.

Climate is represented by three variables (resolution=1-km): climatic moisture deficit (CMD), reference evapotranspiration minus CMD, hereafter referred to as evapotranspiration (ET), and mean summertime temperature (June through August) (T.sm) (Table 1). These variables represent climate normals over the 1981-2000 time period (i.e. they do not vary annually) and were obtained from Wang et al. (2016) (available at https://adaptwest.databasin.org/). CMD and ET are broadly representative of the climatic water balance (climatic water deficit and actual evapotranspiration, respectively) (Stephenson 1990) but are simplifications because they exclude factors such as soil water holding capacity and wind speed in their calculations. As previously mentioned, these climate variables are likely indirect measures of fuel amount and vegetation type through their effect on productivity (e.g. Miller and Urban 1999, Krawchuk et al. 2009). Nevertheless, variables such as these have been identified as strong predictors of wildland fire in numerous studies (Parks et al. 2014c, 2018, Kane et al. 2015, McKenzie and Littell 2017).

The fire weather group is comprised of six gridded variables, three of which represent daily variability (e.g. daily maximum temperature) and three of which represent annual variability (mean temperature for any given year) (Table 1). Our choice to use two temporal resolutions in characterizing fire weather is a result of research that has elucidated the importance of both daily and annual fire weather in driving fire severity (e.g. Abatzoglou et al. 2017, Keyser and Westerling 2017, Lydersen et al. 2017). The daily gridded fire weather variables (resolution=4-km) include burning index (BI.day), energy release component (ERC.day), and maximum temperature (Tmax.day) (Table 1). These weather variables were selected based on recent studies that used daily fire weather in evaluations of fire spread and severity (Collins et al. 2009, Birch et al. 2015, Holsinger et al. 2016). BI.day is related to the potential flame length and ERC.day is a metric of the potential energy released at the head of a spreading fire (Schlobohm and Brain 2002). BI.day and ERC.day were calculated as described by Priesler et al. (2016) and Jolly and Freeborn (2017). To ensure that BI.day and ERC.day were comparable among locations, we constrained calculations to a single fuel model (Fuel Model G), which has a strong relationship with the occurrence of large fires. Tmax.day was obtained from Abatzoglou (2013). Annual fire weather variables (resolution=1-km) include heat moisture (HM.ann), mean temperature (Temp.ann), and climatic moisture deficit (CMD.ann) (Table 1). These variables represent the year in which any given fire occurred and were generated using the ClimateNA software package (version 5.10) (Wang et al. 2016). Several studies have used similar variables in evaluations of fire activity or severity (Parisien et al. 2014, Abatzoglou et al. 2017, Keyser and Westerling 2017).

Table 1. Variables used as predictors in modeling the probability of high-severity fire in forests of the western US.

Group	Variable name	Description	Source
Live fuel	NDVI	Normalized differenced vegetation index. Calculated using pre-fire imagery distributed by the Monitoring Trends in Burn Severity (MTBS) program.	Pettorelli et al. (2005)
	NDMI	Normalized differenced moisture index. Calculated using pre-fire imagery distributed by MTBS (Eidenshink et al. 2007).	McDonald et al. (1998)
	EVI	Enhanced vegetation index. Calculated using pre-fire imagery distributed by MTBS (Eidenshink et al. 2007).	Huete (2002)
Topography	DISS	Dissection index with a 450 meter radius. DISS is a measure of topographic complexity.	Evans (1972)
	TPI	Topographic position index with a 2000 meter radius. TPI is a measure of valley bottom vs. ridge top.	NA
	SRAD	Solar radiation, as calculated using the SOLPET6 model.	Flint et al. (2004)
	Slope	Slope angle	NA
Climate	CMD	Climatic moisture deficit (Wang et al. 2016). Mean over the 1961-1990 time period.	Wang et al. (2016); https://adaptwest.databasin.org/
	ET	Evapotranspiration (i.e. Eref - CMD). Mean over the 1961-1990 time period.	Wang et al. (2016); https://adaptwest.databasin.org/
	T.sm	Average summer temperature. Mean over the 1961-1990 time period.	Wang et al. (2016); https://adaptwest.databasin.org/
Fire weather	BI.day	Burning index; a measure of fire intensity. Raw value converted to per-pixel percentile.	Preisler et al. (2016) Jolly and Freeborn (2017)
	ERC.day	Energy release component; an index describing the amount of heat released per unit area at the flaming front of a fire. Raw value converted to per-pixel percentile.	Preisler et al. (2016) Jolly and Freeborn (2017)
	Tmax.day	Maximum daily temperature. Raw value converted to per-pixel percentile.	Abatzoglou (2013)
	HM.ann	Heat moisture for the year in which the fire occurred. HM is calculated as follows: (annual temperature + 10) / (annual precipitation/1000). Raw value converted to per-pixel z-score.	ClimateNA software package; Wang et al. (2016)
	Temp.ann	Mean annual temperature for the year in which the fire occurred. Raw value converted to per-pixel z-score.	ClimateNA software package; Wang et al. (2016)
	CMD.ann	Climatic moisture deficit for the year in which the fire occurred. Raw value converted to per-pixel z-score.	ClimateNA software package; Wang et al. (2016)

Daily weather variables were converted to daily percentiles based on 25 years of data (1990-2014) and on the estimated fire season for each ecoregion; that is, each 4-km pixel is assigned a daily percentile based on the weather values of that same pixel over the fire seasons from 1990 to 2014. We followed Parks et al. (2016) by defining the fire season for each ecoregion as the date range that encompassed 90% of Moderate Resolution Imaging Spectrometer (MODIS) fire detections from 2002-2014 (USDA Forest Service 2016). To assign a daily weather value for each variable, it was first necessary to identify the day at which each pixel burned. Consequently, we generated fire progression maps using MODIS fire detection data using the methods developed by Parks (Parks 2014). Once the day at which each pixel burned was identified, daily weather percentiles specific to the day of burning were extracted for each burned pixel. Similarly, annual weather variables were converted to z-scores based on the record from 1984-2015 for each 1-km pixel; annual weather z-scores were extracted for the year in which each pixel burned.

Sampling design and statistical models

We sampled individual 30-m pixels within fires that occurred from 2002-2014. Fires that occurred prior to 2002 were not sampled because MODIS data were not available; MODIS data were necessary to estimate day of burning and incorporate daily fire weather into our models. Each ecoregion was modeled separately but included an additional 10 km buffer; the buffer was intended to ensure that adjacent forest was also modeled in cases where ecoregion boundaries are imperfect. We only sampled pixels identified as forest (i.e. forest, woodland, and savanna), as defined by a combination of landscape level vegetation products that include Landfire's (Rollins 2009) Existing Vegetation Cover (EVC), Environmental Site Potential (ESP) and the Landsat Time Series Stacks – Vegetation Change Tracker (LTSS-VCT) (Huang et al. 2010). From the full set of burned forested pixels, we generated an initial 5% random sample, but then removed all pixels <100 m from the fire perimeter to reduce edge effects common at fire boundaries (Stevens-Rumann et al. 2016); this resulted in a ~10% reduction in our samples (Appendix A). Although predictor variables ranged in resolution from 30-m to 4-km, all analyses and predictions were conducted using the native resolution of the response variable (30-m).

For each ecoregion, we used boosted regression trees (BRT) using the 'gbm' package in R to model high-severity fire (binary response) as a function of live fuel, topography, climate, and fire weather (Table 1). To adequately model high-severity fire, we built models only for ecoregions with at least 50,000 samples (this is of the initial 5% sample and excludes samples in the buffer). A handful of ecoregions were consequently omitted because they contained a low proportion of forest or did not have enough fire data (e.g. Sonoran Desert and North Cascades ecoregion, respectively) (Appendix A). BRT models were built using 100,000 randomly selected samples (from the initial 5% random sample) within each ecoregion (plus 10-km buffer). In cases where there were < 100,000 (and ≥ 50,000) available samples, we used all samples (from the initial 5% random sample). BRT parameters were set as follows for each model: learning rate=0.025, number of trees=1000, and tree complexity=2. These parameters were chosen based a) on the recommendations of Elith et al. (2008) and b) those that maximized the cross-validated model fit (described below).

In an effort to reduce overfitting and build the most parsimonious model for each ecoregion, we employed a cross-validated stepwise procedure in which specific variables were removed if they did not

provide unique information that improved model fit. Models for each ecoregion were evaluated with five-fold cross validation that was spatially and temporally structured such that 20% of fires (as opposed to pixels) within an ecoregion were held out in each iteration. Specifically, we built a model for each ecoregion using the full suite of variables (Table 1) and evaluated it with the area under curve (AUC) statistic derived from the receiver operating characteristic curve as measured with the 'verification' package in R; the AUC was averaged over the five folds. We then built an additional set of models for each ecoregion in which each explanatory variable was removed and calculated the AUC as previously described. If the cross-validated AUC *increased* when any given variable was removed from the model, it indicates that the model is overfit and that the variable does not provide any unique information in explaining high-severity fire. In these cases, the variable that resulted in the largest increase in AUC was permanently removed and the process was repeated until all variables resulted in a decreased AUC when removed from the model. As such, all variables in the final models provided unique information in terms of explaining high-severity fire. Given strong autocorrelation in fire severity data (Parks et al. 2014b, Kane et al. 2015), this approach was much more conservative and arguably more appropriate in terms of evaluating model fit compared to validations that do not hold out truly independent data (i.e. data from fires not used to build the models). This approach to variable selection also ensured that our models are spatially and temporally transferable, which is important given our desire to map predictions (objectives 2 and 3).

Once the final model for each ecoregion was identified, the relative importance of variable groups was calculated using the AUC of a five-fold cross validation using a process that excluded all variables from a particular group. Specifically, we compared the five-fold cross validated AUC of the full model to models that iteratively excluded all variables representing live fuel, topography, climate, and fire weather. Relatively small decreases in AUC (compared to the full model) for any particular variable group were interpreted as having less influence compared to variable groups that resulted in larger decreases in AUC. The specific equation was as follows:

$$Relative\ influence_i = \frac{AUC.full - AUC.no.var_i}{\sum_{i=1}^{i=4}(AUC.full - AUC.no.var_i)} \times 100$$

Where *AUC.full* was the AUC of the full model, *AUC.no.var* was the AUC of the model excluding any particular variable group, and *i* represented one of the four variable groups.

Model implementation and map production

From these BRT models, we produced wall-to-wall raster maps (objective 2) depicting the probability of high-severity fire, if a fire were to occur, for each ecoregion in which the cross-validated AUC ≥0.70. We reasoned that the uncertainty in some models (i.e. those with an AUC <0.70) would potentially result in low-quality maps because the prevalence of true-positives is not much greater than the false positives when AUC <0.70 (Swets 1988). For the fuel inputs (NDVI, NDMI, and EVI), satellite imagery from 2016 spanning the entirety of each ecoregion was obtained using Google Earth Engine (GEE; https://developers.google.com/earth-engine/). Consequently, these raster predictions represent fairly current fuel conditions across each ecoregion. Predictions theoretically range from zero to one and depicted the probability of high-severity fire.

We aimed to produce these severity predictions representing the average weather conditions under which fires burn. This is somewhat challenging, however, given that weather is spatially and temporally dynamic. Consequently, we produced 100 initial predictions and varied the weather for each of these predictions; all other inputs across each ecoregion (fuel from 2016, topography, and climate) were held static. To vary the weather, we randomly selected 100 records from our fire severity datasets. Each record represents one burned pixel with a unique combination of daily and annual fire weather; this approach preserved the covariance among the observed fire weather variables. We used the observed fire weather from each random record for each of the 100 initial predictions. Each weather value was assigned to the entire ecoregion for each of the 100 initial predictions. We then averaged the 100 initial predictions over each 30-m pixel, resulting in one raster map depicting the probability of high-severity fire under average weather conditions in which fires burn. An important consideration here is that the severity predictions do not represent 'average weather conditions', but the 'average weather conditions *under which fire burn'.* That is, because fires often burn under more extreme fire weather, our predictions implicitly incorporate weather associated with high fire activity. This consideration also pertains to our mapped predictions under moderate and extreme fire weather, as described in the next paragraph. For those ecoregions in which the relative importance of weather was zero (n=2; but see Discussion), the process was much simpler since we only needed one prediction using fuel from 2016, topography, and climate as inputs.

For those ecoregions in which the relative influence of fire weather ≥15%, we produced two additional raster maps, one depicting the probability of high-severity fire under conditions representing moderate weather and the other under conditions representing extreme weather. To do so, we calculated the 50^{th} and 95^{th} percentile *for each pixel* out of the 100 previously described initial predictions. While these maps represent the 50^{th} and 95^{th} percentile in predicted outcomes for each pixel, we use them to represent the outcomes of moderate and extreme fire weather, respectively. Neither says anything specific about the percentile of weather conditions under which they occurred, but they can be interpreted as resulting from moderate and extreme fire weather conditions. We did not produce mapped predictions under conditions representing moderate and extreme weather when the relative influence fire weather was <15% because we would not expect to see substantial differences between the two predictions. Said another way, if fire weather has a fairly low relative importance, it is not prudent to produce maps under various weather scenarios.

While it would be ideal to use specific percentiles of our fire weather variables to represent moderate vs. extreme conditions, we could not do this because of complex interactions among them. For example, extreme fire behavior is known to occur during periods of high temperature, but may also occur during periods of low temperature but high winds (resulting in high BI.day); this is fairly common when cold fronts pass through a region. Furthermore, some fire weather variables may be more important in particular ecoregions, and a detailed assessment of individual weather variables was beyond the scope of this study. We felt that using randomized weather observations, which preserved the covariance among the observed fire weather variables, along with the 50^{th} and 95^{th} percentile high-severity fire predictions, provided for an unbiased and consistent approach to modelling severity representative of moderate and extreme fire weather. This approach is similar to that of Finney et al. (2011).

To illustrate how our models can potentially be used to monitor changes in the probability of high-severity fire due to fuel treatments (objective 3), we made pre- and post-treatment predictions using the BRT model from the Arizona – New Mexico Mountains ecoregion. We obtained imagery representing the live fuel variables using GEE for the years 2007 (pre-treatment) and 2011 (post-treatment); fuel treatment data (location and type) were obtained from Landfire (Rollins 2009; www.landfire.gov). Again, we produced two sets of predictions for each time period (pre- and post-treatment) representing moderate and extreme fire weather, as previously described.

Literature cited

Abatzoglou, J. T. 2013. Development of gridded surface meteorological data for ecological applications and modelling. International Journal of Climatology 33:121–131.

Abatzoglou, J. T., C. A. Kolden, A. P. Williams, J. A. Lutz, and A. M. S. Smith. 2017. Climatic influences on interannual variability in regional burn severity across western US forests. International Journal of Wildland Fire 26:269–275.

Birch, D. S., P. Morgan, C. A. Kolden, J. T. Abatzoglou, G. K. Dillon, A. T. Hudak, and A. M. S. Smith. 2015. Vegetation, topography and daily weather influenced burn severity in central Idaho and western Montana forests. Ecosphere 6:art17.

Chu, T., X. Guo, and K. Takeda. 2016. Temporal dependence of burn severity assessment in Siberian larch (Larix sibirica) forest of northern Mongolia using remotely sensed data. International Journal of Wildland Fire 25:685–698.

Collins, B. M., J. D. Miller, A. E. Thode, M. Kelly, J. W. van Wagtendonk, and S. L. Stephens. 2009. Interactions Among Wildland Fires in a Long-Established Sierra Nevada Natural Fire Area. Ecosystems 12:114–128.

Dillon, G. K., Z. A. Holden, P. Morgan, M. A. Crimmins, E. K. Heyerdahl, and C. H. Luce. 2011. Both topography and climate affected forest and woodland burn severity in two regions of the western US, 1984 to 2006. Ecosphere 2:art130.

Eidenshink, J. C., B. Schwind, K. Brewer, Z.-L. Zhu, B. Quayle, and S. M. Howard. 2007. A project for monitoring trends in burn severity. Fire ecology 3:3–21.

Elith, J., J. R. Leathwick, and T. Hastie. 2008. A working guide to boosted regression trees. Journal of Animal Ecology 77:802–813.

Evans, I. S. 1972. General geomorphometry, derivatives of altitude, and descriptive statistics. Spatial analysis in geomorphology:17–90.

Finney, M. A., I. C. Grenfell, C. W. McHugh, R. C. Seli, D. Trethewey, R. D. Stratton, and S. Brittain. 2011. A Method for Ensemble Wildland Fire Simulation. Environmental Modeling & Assessment 16:153–167.

Flint, A. L., L. E. Flint, J. A. Hevesi, and J. B. Blainey. 2004. Fundamental concepts of recharge in the desert southwest: A regional modeling perspective. Pages 159–184. American Geophysical Union.

Holsinger, L., S. A. Parks, and C. Miller. 2016. Weather, fuels, and topography impede wildland fire spread in western US landscapes. Forest Ecology and Management 380:59–69.

Huang, C., S. N. Goward, J. G. Masek, N. Thomas, Z. Zhu, and J. E. Vogelmann. 2010. An automated approach for reconstructing recent forest disturbance history using dense Landsat time series

stacks. Remote Sensing of Environment 114:183–198.
Huete, A., K. Didan, T. Miura, E. P. Rodriguez, X. Gao, and L. G. Ferreira. 2002. Overview of the radiometric and biophysical performance of the MODIS vegetation indices. Remote Sensing of Environment 83:195–213.
Jolly, W. M., and P. H. Freeborn. 2017. Towards improving wildland firefighter situational awareness through daily fire behaviour risk assessments in the US Northern Rockies and Northern Great Basin. International Journal of Wildland Fire 26:574–586.
Kane, V. R., C. A. Cansler, N. A. Povak, J. T. Kane, R. J. McGaughey, J. A. Lutz, D. J. Churchill, and M. P. North. 2015. Mixed severity fire effects within the Rim fire: Relative importance of local climate, fire weather, topography, and forest structure. Forest Ecology and Management 358:62–79.
Key, C. H. 2006. Ecological and sampling constraints on defining landscape fire severity. Fire Ecology 2:34–59.
Keyser, A., and A. Westerling. 2017. Climate drives inter-annual variability in probability of high severity fire occurrence in the western United States. Environmental Research Letters.
Krawchuk, M. A., M. A. Moritz, M. A. Parisien, J. Van Dorn, and K. Hayhoe. 2009. Global pyrogeography: The current and future distribution of wildfire. PLoS ONE 4:5102.
Lydersen, J. M., B. M. Collins, M. L. Brooks, J. R. Matchett, K. L. Shive, N. A. Povak, V. R. Kane, and D. F. Smith. 2017. Evidence of fuels management and fire weather influencing fire severity in an extreme fire event. Ecological Applications 27:2013–2030.
McDonald, A. J., F. M. Gemmell, and P. E. Lewis. 1998. Investigation of the utility of spectral vegetation indices for determining information on coniferous forests. Remote Sensing of Environment 66:250–272.
McKenzie, D., and J. S. Littell. 2017. Climate change and the eco-hydrology of fire: Will area burned increase in a warming western USA? Ecological applications 27:26–36.
Miller, C., and D. L. Urban. 1999. A model of surface fire, climate and forest pattern in the Sierra Nevada, California. Ecological Modelling 114:113–135.
Miller, J. D., E. E. Knapp, C. H. Key, C. N. Skinner, C. J. Isbell, R. M. Creasy, and J. W. Sherlock. 2009. Calibration and validation of the relative differenced Normalized Burn Ratio (RdNBR) to three measures of fire severity in the Sierra Nevada and Klamath Mountains, California, USA. Remote Sensing of Environment 113:645–656.
Olson, D. M., and E. Dinerstein. 2002. The Global 200: Priority ecoregions for global conservation. Annals of the Missouri Botanical garden:199–224.
Parisien, M.-A., S. A. Parks, M. A. Krawchuk, J. M. Little, M. D. Flannigan, L. M. Gowman, and M. A. Moritz. 2014. An analysis of controls on fire activity in boreal Canada: Comparing models built with different temporal resolutions. Ecological Applications 24.
Parks, S. A. 2014. Mapping day-of-burning with coarse-resolution satellite fire-detection data. International Journal of Wildland Fire 23:215–223.
Parks, S. A., G. K. Dillon, and C. Miller. 2014a. A new metric for quantifying burn severity: the relativized burn ratio. Remote Sensing 6:1827–1844.
Parks, S. A., L. M. Holsinger, C. Miller, and M.-A. Parisien. 2018. Analog-based fire regime and vegetation shifts in mountainous regions of the western US. Ecography in press.
Parks, S. A., C. Miller, L. M. Holsinger, L. S. Baggett, and B. J. Bird. 2016. Wildland fire limits subsequent fire occurrence. International Journal of Wildland Fire 25:182–190.

Parks, S. A., C. Miller, C. R. Nelson, and Z. A. Holden. 2014b. Previous Fires Moderate Burn Severity of Subsequent Wildland Fires in Two Large Western US Wilderness Areas. Ecosystems 17:29–42.

Parks, S. A., M. A. Parisien, C. Miller, and S. Z. Dobrowski. 2014c. Fire activity and severity in the western US vary along proxy gradients representing fuel amount and fuel moisture. PLoS ONE 9:e99699.

Pettorelli, N., J. O. Vik, A. Mysterud, J.-M. Gaillard, C. J. Tucker, and N. C. Stenseth. 2005. Using the satellite-derived NDVI to assess ecological responses to environmental change. Trends in ecology & evolution 20:503–510.

Preisler, H. K., K. L. Riley, C. S. Stonesifer, D. E. Calkin, and W. M. Jolly. 2016. Near-term probabilistic forecast of significant wildfire events for the Western United States. International Journal of Wildland Fire 25:1169–1180.

Rollins, M. G. 2009. LANDFIRE: a nationally consistent vegetation, wildland fire, and fuel assessment. International Journal of Wildland Fire 18:235–249.

Schlobohm, P., and J. Brain. 2002. Gaining an understanding of the national fire danger rating system. National Wildfire Coordinating Group, PMS 932.

Stephenson, N. L. 1990. Climatic control of vegetation distribution: the role of the water balance. American Naturalist:649–670.

Stevens-Rumann, C., S. Prichard, E. Strand, and P. Morgan. 2016. Prior wildfires influence burn severity of subsequent large fires. Canadian Journal of Forest Research 46:1375–1385.

Swets, J. A. 1988. Measuring the accuracy of diagnostic systems. Science 240:1285–1293.

Turner, M. G. 2010. Disturbance and landscape dynamics in a changing world. Ecology 91:2833–2849.

USDA Forest Service. 2016. MODIS fire detection GIS data.

Wang, T., A. Hamann, D. Spittlehouse, and C. Carroll. 2016. Locally downscaled and spatially customizable climate data for historical and future periods for North America. PLOS ONE 11:e0156720.